J Therm Anal Calorim (2012) 110:949–954
DOI 10.1007/s10973-011-1889-7

Heat capacities and thermodynamic properties of M(HBTC)(4,4′-bipy)·3DMF (M = Ni and Co)

Yi-Xi Zhou · Li-Xian Sun · Zhong Cao · Jian Zhang · Fen Xu · Li-Fang Song · Zi-Ming Zhao · Yong-Jin Zou

Received: 21 July 2011 / Accepted: 25 August 2011 / Published online: 9 September 2011

Abstract Two metal–organic frameworks (MOFs) of M(HBTC)(4,4′-bipy)·3DMF [M = Ni (for **1**) and Co (for **2**); H_3BTC = 1,3,5-benzenetricarboxylic acid (1,3,5-BTC); 4,4′-bipy = 4,4′-bipyridine; DMF = *N*,*N*′-dimethylformamide] were synthesized by a one-pot solution reaction and a solvothermal method, respectively, and characterized by powder X-ray diffraction and FT-IR spectra. The low-temperature molar heat capacities of M(HBTC)(4,4′-bipy)·3DMF were measured by temperature-modulated differential scanning calorimetry (TMDSC) for the first time. The thermodynamic parameters such as entropy and enthalpy relative to reference temperature 298.15 K were derived based on the above molar heat capacity data. Moreover, the thermal stability and the decomposition mechanism of M(HBTC)(4,4′-bipy)·3DMF were investigated by thermogravimetry analysis (TGA). The experimental results through TGA measurement demonstrate that both of the two compounds have a three-stage mass loss in air flow.

Y.-X. Zhou · Z. Cao (✉)
School of Chemistry and Biological Engineering, Changsha University of Science and Technology, Changsha 410004, People's Republic of China
e-mail: zhongcao04@yahoo.com.cn

Y.-X. Zhou · L.-X. Sun (✉) · J. Zhang · L.-F. Song · Z.-M. Zhao · Y.-J. Zou
Materials and Thermochemistry Laboratory, Dalian Institute of Chemical Physics, Chinese Academy of Sciences, Dalian 116023, People's Republic of China
e-mail: lxsun@dicp.ac.cn

F. Xu
Faculty of Chemistry and Chemical Engineering, Liaoning Normal University, Dalian 116029, People's Republic of China

Keywords Metal–organic framework · Molar heat capacity · TGA · TMDSC

Introduction

Nowadays, a new class of crystalline materials which possess low density and high surface areas called metal–organic frameworks (MOFs) have been widely developed and synthesized [1]. These materials are molecular architectures constructed by metal ions and organic ligands. Many of them have so good properties that can be applied as new functional materials for gas storage [2], gas separation [3], chemical sensor [4], biological analysis [5], and so on. However, there is little research on their thermodynamic properties.

The aromatic carboxylic acids and the bipyridine ligands are widely used polyfunctional organic linkers to form mixed-ligands frameworks. The aromatic carboxylic acids, such as 1,4-benzenedicarboxylic acid (1,4-BDC), 1,3,5-benzenetricarboxylic acid (1,3,5-BTC), have been widely used as bridging ligands for design and synthesis of porous materials with stable structures and high porosity. The bipyridine ligands are able to combine with different aromatic carboxylate co-ligands to assemble into varied polymeric frameworks consisting of one-, two- or three-dimensional structures [6].

Molar heat capacities of MOFs at different temperatures have received considerable attention as basic data in chemistry and engineering, from which many other thermodynamic parameters such as enthalpy and entropy can be calculated [7]. These parameters are very important for both theoretical and practical purposes.

Temperature-modulated differential scanning calorimetry (TMDSC) is one easy and accurate method for

determining heat capacity [8]. The structure and principle of the calorimeter have been described in references [9–11]. Nowadays, this method has been fully developed for directly determining heat capacities for a large number of materials [12–14].

In the present article, we have selected two MOFs materials, namely Ni(HBTC)(4,4′-bipy)·3DMF (**1**) and Co(HBTC)(4,4′-bipy)·3DMF (**2**). Compounds **1** and **2** were synthesized by a one-pot solution reaction and a solvothermal method, respectively, by slightly modifying the literature recipe [15, 16]. Their structures were characterized by powder X-ray diffraction and FT-IR spectra. Their thermal decomposition patterns were investigated by thermogravimetry analysis (TGA), and their molar heat capacities were measured by TMDSC.

Experimental

All reagents were purchased commercially and used without further purification.

Sample preparation

Ni(HBTC)(4,4′-bipy)·3DMF was prepared by a mild solution method. A solution of H_3BTC (H_3BTC = 1,3,5-BTC; 0.21 g, 1 mmol), 4,4′-bipy (4,4′-bipy = 4,4′-bipyridine; 0.19 g, 1 mmol), and $Ni(NO_3)_2{\cdot}6H_2O$ (0.29 g, 1 mmol) in 40 mL of DMF was kept in a glass conical flask and heated at 393 K for 4 h. After being filtered and thoroughly washed by DMF and C_2H_5OH, the obtained green crystals were dried in air at 323 K for 24 h before other measurements. The yield of Ni(HBTC)(4,4′-bipy)·3DMF was 73%.

Co(HBTC)(4,4′-bipy)·3DMF was prepared by a solvothermal method. A solution of H_3BTC (H_3BTC = 1,3,5-BTC; 0.21 g, 1 mmol), 4,4′-bipy (4,4′-bipy = 4,4′-bipyridine; 0.19 g, 1 mmol), and $Co(NO_3)_2{\cdot}6H_2O$ (0.29 g, 1 mmol) in 20 mL DMF was sealed in a 40 mL Teflon-lined autoclave and heated at 353 K for 72 h. The resultant red powders were washed with DMF and C_2H_5OH. The yield of Co(HBTC)(4,4′-bipy)·3DMF was 53%.

Characterization

FT-IR spectra were recorded on a Nicolet 380 FT-IR spectrometer using KBr pellet in the wavenumber range of 4,000–400 cm^{-1}. Powder X-ray diffraction (PXRD) patterns were measured on a X'Pert PRO X-ray diffractometer using Cu Kα radiation (40 kV, 40 mA).

The PXRD patterns of the as-synthesized two compounds and their simulated patterns are shown in Fig. 1. Figure 1 indicates that diffraction peaks of the samples

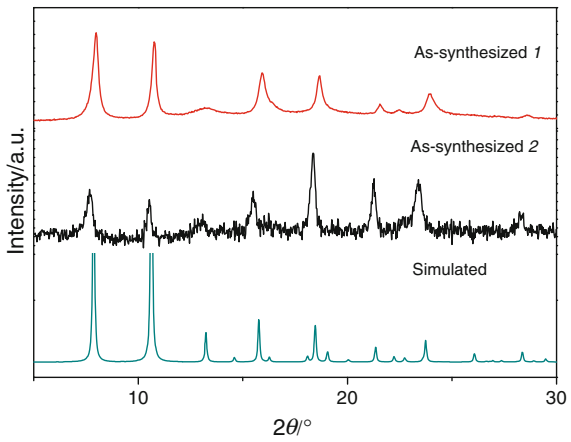

Fig. 1 PXRD patterns of as-synthesized and simulated for **1** and **2**

prepared in this study match well with the simulated pattern according to the published article [15]. It confirms that the samples have high purity.

FT-IR for **1**: 3,392 cm^{-1}, ν(O–H); 3,100 cm^{-1}, ν_s(C–H); 1,647–1,369 cm^{-1}, ν(aromatic C=C); 813–717 cm^{-1}, ν_s (aromatic C–H); for **2**: 3,390 cm^{-1}, ν(O–H); 3,083 cm^{-1}, ν_s(C–H); 1,659–1,371 cm^{-1}, ν(aromatic C=C); 813–717 cm^{-1}, and ν_s(aromatic C–H).

Thermal analysis

TGA was carried out on a Cahn Thermax 500 from room temperature to 873 K in air flow. The heating rate was 5 K min^{-1} and the flow rate of air was 100 mL min^{-1}. The TGA equipment was calibrated by the $CaC_2O_4{\cdot}H_2O$ (99.9%). The mass of the compounds were 46.80 mg (**1**) and 65.02 mg (**2**).

Heat capacity measurement

Heat capacity measurements of the two samples were performed on a DSC Q1000 (T-zero DSC-technology, TA Instruments Inc., USA). A mechanical cooling system was used for the experimental measurement. Dry nitrogen gas with high purity (99.999%) was used as purge gas (50 mL min^{-1}) through the DSC cell. The temperature scale of the instrument was initially calibrated in the standard DSC mode, using the extrapolated onset temperatures of the melting of indium (429.75 K) at a heating rate of 10 K min^{-1}. The energy scale was calibrated with the heat of fusion of indium (28.45 J g^{-1}). The heat capacity calibration was made by running a standard sapphire (α-Al_2O_3) at the experimental temperature. The calibration method was performed at the conditions as follows: (1) sampling interval: 1.00 s/pt; (2) equilibrate at 183.15 K; (3) isothermal for 5.00 min; and (4) temperature ramp at 10 K min^{-1}–303.15 K.

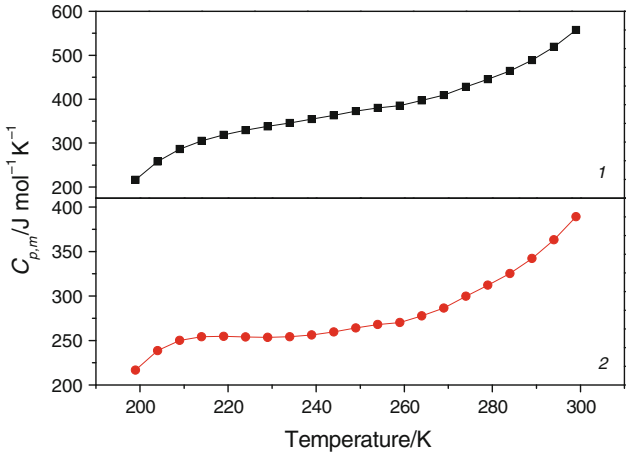

Fig. 2 Molar heat capacities ($C_{p,m}$) of **1** and **2** as a function of temperature

Samples were crimped in hermetically sealed aluminum pans with lids using TA's Blue DSC Sample Press. Sample mass was weighed on a METTLER TOLEDO analytical balance (AB135-S, Classic Plus). The masses of the reference and sample pans with lids were within 57.33 ± 0.05 mg.

Results and discussion

Heat capacity of standard sapphire (α-Al_2O_3)

Heat capacity measurements were repeated three times unless stated elsewhere. The emphasis of this study is to assess the reproducibility and ensure accuracy of the measured data using TMDSC (Q1000). The experimental standard deviation is during ±0.2% and the result shows that the testing system of TMDSC is steady. Relative deviations have been calculated by the following equation:

$$\mathrm{RD}(\%) = 100\left[C_{p,m}(\mathrm{exp}) - C_{p,m}(\mathrm{ref})\right]/C_{p,m}(\mathrm{ref}) \qquad (1)$$

where $C_{p,m}$(exp) is the average experimental heat capacities and $C_{p,m}$(ref) is the referenced heat capacities. The results show that the relative deviation of our calibration data from the recommended value [17] was within ±1.4% over the whole temperature range.

Heat capacity

The average experimental molar heat capacities curve of **1** and **2** versus temperature are shown in Fig. 2. It can be seen that the heat capacities of the compounds increase with temperature continuously in the temperature range from 199 to 299 K. No phase transition or thermal anomaly was observed in the experimental temperature range. It

Table 1 The data of three reduplicate experiments for **1**

T/K	$C_{p,m}$(exp)/J K^{-1} g^{-1}				Standard deviation
	a	*b*	*c*	Average	
199	0.3273	0.3876	0.2962	0.3370	0.0465
204	0.4019	0.4393	0.3642	0.4018	0.0376
209	0.4514	0.4740	0.4133	0.4462	0.0307
214	0.4827	0.4965	0.4474	0.4755	0.0253
219	0.5033	0.5126	0.4730	0.4963	0.0207
224	0.5181	0.5261	0.4943	0.5128	0.0165
229	0.5285	0.5375	0.5126	0.5262	0.0126
234	0.5382	0.5479	0.5304	0.5388	0.0088
239	0.5480	0.5590	0.5485	0.5518	0.0062
244	0.5577	0.5704	0.5677	0.5653	0.0067
249	0.5692	0.5834	0.5893	0.5806	0.0103
254	0.5778	0.5932	0.6060	0.5923	0.0141
259	0.5808	0.6004	0.6185	0.5999	0.0189
264	0.596	0.6200	0.6391	0.6184	0.0216
269	0.6123	0.6406	0.6599	0.6376	0.0239
274	0.6400	0.6686	0.6903	0.6663	0.0252
279	0.6663	0.6996	0.7155	0.6938	0.0251
284	0.6943	0.7335	0.7407	0.7228	0.0250
289	0.7323	0.7803	0.7703	0.7610	0.0253
294	0.7815	0.8407	0.8030	0.8084	0.0300
299	0.8447	0.9203	0.8389	0.8680	0.0454

Table 2 The data of three reduplicate experiments for **2**

T/K	$C_{p,m}$(exp)/J K^{-1} g^{-1}				Standard deviation
	a	*b*	*c*	Average	
199	0.3373	0.3226	0.3521	0.3373	0.0148
204	0.3691	0.3624	0.3832	0.3716	0.0106
209	0.3868	0.3828	0.3979	0.3892	0.0078
214	0.3949	0.3892	0.4024	0.3955	0.0066
219	0.3986	0.3884	0.4023	0.3964	0.0072
224	0.4003	0.3846	0.4011	0.3953	0.0093
229	0.4021	0.3809	0.4004	0.3945	0.0118
234	0.4058	0.3792	0.4019	0.3956	0.0144
239	0.4116	0.3797	0.4056	0.3990	0.0170
244	0.4192	0.3816	0.4112	0.4040	0.0198
249	0.4293	0.3852	0.4188	0.4111	0.0230
254	0.4370	0.3883	0.4262	0.4172	0.0256
259	0.4424	0.3882	0.4310	0.4205	0.0286
264	0.4552	0.3975	0.4434	0.4320	0.0305
269	0.4696	0.4116	0.4563	0.4458	0.0304
274	0.4946	0.4329	0.4721	0.4665	0.0312
279	0.5121	0.4559	0.4895	0.4858	0.0283
284	0.5302	0.4812	0.5075	0.5063	0.0245
289	0.5535	0.5158	0.5289	0.5327	0.0191
294	0.5816	0.5605	0.5538	0.5653	0.0145
299	0.6149	0.6191	0.5836	0.6059	0.0194

indicates that the compounds are stable in this temperature region.

The data of three reduplicate experiments and the experimental standard deviation for **1** and **2** are given in Tables 1 and 2. The experimental standard deviations below 4.7 and 3.1% are obtained. The experimental and simulated molar heat capacities data are listed in Tables 3 (for **1**) and 4 (for **2**).

The molar heat capacities of the samples are fitted to the following polynomial equation of heat capacities ($C_{p,m}$) with reduced temperature (X) using the Origin Pro 7.5 software:

From $T = (199–299)$ K (for **1**)

$$C_{p,m,1}\left(\text{J mol}^{-1}\text{ K}^{-1}\right) = 369.5 + 83.76X + 43.10X^2 + 36.32X^3 - 24.84X^4 + 49.85X^5 \quad (2)$$

From $T = (199–299)$ K (for **2**)

$$C_{p,m,2}\left(\text{J mol}^{-1}\text{ K}^{-1}\right) = 261.2 + 41.54X + 71.57X^2 - 5.042X^3 - 28.90X^4 + 49.34X^5 \quad (3)$$

where $X = (T - 249)/50$, and T is the experimental temperature, 249 is obtained from polynomial $(T_{max} + T_{min})/2$, 50 is obtained from polynomial $(T_{max} - T_{min})/2$, T_{max} is the upper limit of the above temperature region, T_{min} is the lower limit of the above temperature region. The correlation coefficients are: $R^2 = 0.99961$ (for **1**) and 0.99877 (for **2**). The relative deviations of all the experimental points from the fitting heat capacities values are within ±0.92% (for **1**) in Table 3 and ±1.1% (for **2**) in Table 4. Based on Eq. 2, the molar heat capacity of **1** at 298.15 K was calculated to be 550.5 J mol^{-1} K^{-1}, and based on Eq. 3, the molar heat capacity of **2** at 298.15 K was calculated to be 384.7 J mol^{-1} K^{-1}.

Thermodynamic functions

Enthalpy and entropy of substances are basic thermodynamic functions. In terms of the polynomials of molar heat capacity and the thermodynamic relationship, the $[H_T - H_{298.15}]$ and $[S_T - S_{298.15}]$ of **1** and **2** are calculated with an

Table 3 The experimental and simulated molar heat capacities of **1**

T/K	$C_{p,m}$(exp)/J K^{-1} mol^{-1}	$C_{p,m}$(fit)/J K^{-1} mol^{-1}	RD/%	T/K	$C_{p,m}$(exp)/J K^{-1} mol^{-1}	$C_{p,m}$(fit)/J K^{-1} mol^{-1}	RD/%
199	216.5	217.8	0.63	254	380.4	378.3	−0.55
204	258.1	256.8	−0.49	259	385.3	388.2	0.76
209	286.6	285.0	−0.57	264	397.2	399.4	0.56
214	305.4	305.2	−0.08	269	409.5	412.1	0.63
219	318.8	319.8	0.33	274	428.0	426.7	−0.29
224	329.4	330.7	0.41	279	445.6	443.8	−0.41
229	338.0	339.4	0.43	284	464.3	464.1	−0.03
234	346.1	346.9	0.25	289	488.8	488.8	0.02
239	354.4	354.1	−0.09	294	519.2	519.4	0.04
244	363.1	361.5	−0.43	299	557.5	557.7	0.04
249	372.9	369.5	−0.92				

Table 4 The experimental and simulated molar heat capacities of **2**

T/K	$C_{p,m}$(exp)/J K^{-1} mol^{-1}	$C_{p,m}$(fit)/J K^{-1} mol^{-1}	RD/%	T/K	$C_{p,m}$(exp)/J K^{-1} mol^{-1}	$C_{p,m}$(fit)/J K^{-1} mol^{-1}	RD/%
199	216.7	218.0	0.59	254	268.0	266.1	−0.74
204	238.7	237.4	−0.58	259	270.2	272.3	0.78
209	250.1	248.3	−0.68	264	277.6	279.9	0.81
214	254.1	253.7	−0.17	269	286.5	288.7	0.78
219	254.7	255.5	0.33	274	299.8	299.0	−0.26
224	254.0	255.6	0.63	279	312.2	310.9	−0.41
229	253.5	255.1	0.65	284	325.3	325.0	−0.10
234	254.2	255.0	0.30	289	342.3	342.0	−0.09
239	256.3	255.7	−0.24	294	363.2	363.1	−0.05
244	259.6	257.8	−0.70	299	389.3	389.7	0.11
249	264.1	261.2	−1.11				

Table 5 Calculated thermodynamic function data of **1**

T/K	$H_T - H_{298.15}$/kJ mol^{-1}	$S_T - S_{298.15}$/J K^{-1} mol^{-1}	T/K	$H_T - H_{298.15}$/kJ mol^{-1}	$S_T - S_{298.15}$/J K^{-1} mol^{-1}
199	−37.42	−149.20	254	−19.57	−71.70
204	−36.23	−143.49	259	−17.65	−64.20
209	−34.87	−137.10	264	−15.69	−56.62
214	−33.39	−130.26	269	−13.66	−48.92
219	−31.83	−123.17	274	−11.56	−41.10
224	−30.20	−115.92	279	−9.39	−33.11
229	−28.53	−108.61	284	−7.12	−24.92
234	−26.81	−101.27	289	−4.74	−16.46
239	−25.06	−93.91	294	−2.22	−7.65
244	−23.27	−86.54	298.15	0	0
249	−21.44	−79.14	299	0.47	1.61

Table 6 Calculated thermodynamic function data of **2**

T/K	$H_T - H_{298.15}$/kJ mol^{-1}	$S_T - S_{298.15}$/J K^{-1} mol^{-1}	T/K	$H_T - H_{298.15}$/kJ mol^{-1}	$S_T - S_{298.15}$/J K^{-1} mol^{-1}
199	−27.60	−111.04	254	−13.70	−49.51
204	−26.45	−105.37	259	−12.36	−44.27
209	−25.24	−99.48	264	−10.98	−38.99
214	−23.98	−93.54	269	−9.56	−33.65
219	−22.71	−87.64	274	−8.09	−28.23
224	−21.43	−81.86	279	−6.56	−22.72
229	−20.15	−76.22	284	−4.98	−17.07
234	−18.88	−70.71	289	−3.31	−11.26
239	−17.60	−65.31	294	−1.55	−5.23
244	−16.32	−60.01	298.15	0	0
249	−15.02	−54.75	299	0.33	1.10

interval of 5 K relative to the temperature of 298.15 K. The thermodynamic relationships are as follows:

$$H_T - H_{298.15} = \int_{298.15}^{T} C_{p,m}\mathrm{d}T \quad (4)$$

$$S_T - S_{298.15} = \int_{298.15}^{T} \left(C_{p,m}/T\right)\mathrm{d}T \quad (5)$$

The calculated thermodynamic functions $[H_T - H_{298.15}]$ and $[S_T - S_{298.15}]$ are shown in Tables 5 (for **1**) and 6 (for **2**).

Thermal stabilities and decomposition of **1** and **2**

TGA curve (Fig. 3) of **1** shows a three-stage mass loss in the temperature range from 298 to 873 K. The first mass loss starts at about 305 K and is about 11.6% (calculated 11.4%), which is assigned to the loss of the one DMF molecule in the framework. Further decomposition occurs in the region of 398–668 K and is about 19.1% (calculated

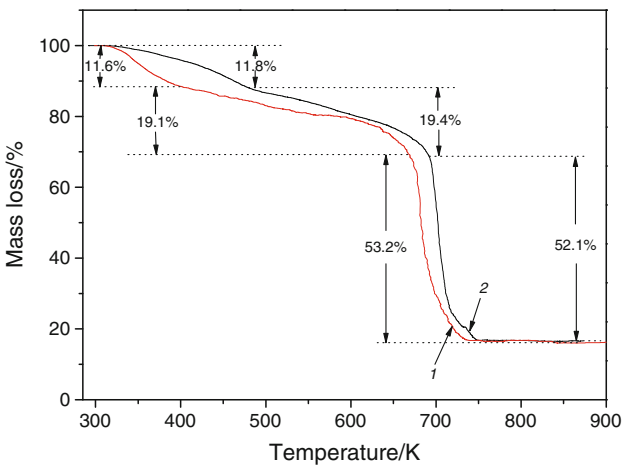

Fig. 3 TGA curves of **1** and **2** under air atmosphere at 5 K min^{-1}

22.7%) according to the degradation of the other DMF molecules. The third loss between 668 and 873 K is about 53.2%, ascribed to the degradation of the 1,3,5-BTC and 4,4′-bipyridine ligands, which means the degradation of the

framework. The overall mass loss of **1** is 83.9% corresponding to NiO as the final residue (calculated 88.4%).

The decomposition of **2** occurs between 292 and 873 K in three steps (Fig. 3). The first mass loss starts at about 308 K and is achieved to 11.8% (calculated 11.4%) at 499 K, which is attributed to the loss of the one DMF molecule. From 499 to 683 K, the second loss corresponds to loss of the other DMF molecules and is about 19.4% (calculated 22.7%). The third stage takes place between 683 and 873 K which means the degradation of the 1,3,5-BTC and 4,4′-bipyridine ligands. The overall mass loss of **2** is about 83.3%, in accord with the calculated percentage (88.3%) for CoO as the final residue.

Conclusions

In this study, two microporous MOFs, Ni(HBTC)(4,4′-bipy)·3DMF (**1**), and Co(HBTC)(4,4′-bipy)·3DMF (**2**), have been synthesized and characterized by powder X-ray diffraction and FT-IR spectra. The molar heat capacities of the compounds were measured using TMDSC for the first time. The heat capacities of the samples at 298.15 K were calculated to be 550.5 (**1**) and 384.7 J mol^{-1} K^{-1} (**2**). The thermodynamic function data relative to the reference temperature 298.15 K were calculated based on the heat capacities measurements. Moreover, both of the two samples reveal a three stages way of decomposition.

Acknowledgements The authors wish to acknowledge the financial support from the National Basic Research Program (973 program) of China (2010CB631303), the National Natural Science Foundation of China (No. 20833009, 20873148, 20903095, 50901070, 51071146, 51071081, and U0734005), National Natural Science Foundation of Liaoning (No. 20102224), Liaoning BaiQianWan Talents Program (Project No. 2010921050), IUPAC (Project No. 2008-006-3-100), The Joint Project of Guangdong Province and Chinese Academy of Sciences (2010A090100034), Dalian Scientific Project (2009A11GX052) and the State Key Laboratory of Explosion Science and Technology, Beijing Institute of Technology (Grant No. KFJJ10-1Z).

References

1. Deng HX, Doonan CJ, Furukawa H, Ferreira RB, Towne J, Knobler CB, Wang B, Yaghi OM. Multiple functional groups of varying ratios in metal-organic frameworks. Science. 2010;327:846–50.
2. Millward AR, Yaghi OM. Metal-organic frameworks with exceptionally high capacity for storage of carbon dioxide at room temperature. J Am Chem Soc. 2005;127:17998–9.
3. Snurr RQ, Bae YS, Spokoyny AM, Farha OK, Hupp JT, Mirkin CA. Separation of gas mixtures using Co(II) carborane-based porous coordination polymers. Chem Commun. 2010;46:3478–80.
4. Kreno LE, Hupp JT, Van Duyne RP. Metal-organic framework thin film for enhanced localized surface plasmon resonance gas sensing. Anal Chem. 2010;82:8042–6.
5. Lee J, Farha OK, Roberts J, Scheidt KA, Nguyen ST, Hupp JT. Metal-organic framework materials as catalysts. Chem Soc Rev. 2009;38:1450–9.
6. Song LF, Jiang CH, Jiao CL, Zhang J, Sun LX, Xu F, Jiao QZ, Xing YH, Du Y, Cao Z, Huang FL. Heat capacities and thermodynamic properties of one manganese-based MOFs. J Therm Anal Calorim. 2010;102:1161–6.
7. Wunderlich B. The tribulations and successes on the road from DSC to TMDSC in the 20th century the prospects for the 21st century. J Therm Anal Calorim. 2004;78:7–31.
8. Androsch R. Heat capacity measurements using temperature-modulated heat flux DSC with close control of the heater temperature. J Therm Anal Calorim. 2000;61:75–89.
9. Wunderlich B. The contributions of MDSC to the understanding of the thermodynamics of polymers. J Therm Anal Calorim. 2006;85:179–87.
10. Divi S, Chellappa R, Chandra D. Heat capacity measurement of organic thermal energy materials. J Chem Thermodyn. 2006;38:1312–26.
11. Danley RL. New modulated DSC measurement technique. Thermochim Acta. 2003;402:91–8.
12. Qiu SJ, Chu HL, Zhang J, Qi YN, Sun LX, Xu F. Heat capacities and thermodynamic properties of CoPc and CoTMPP. J Therm Anal Calorim. 2008;91:841–8.
13. Zhang J, Liu YY, Zeng JL, Xu F, Sun LX, You WS, et al. Thermodynamic properties and thermal stability of the synthetic zinc formate dihydrate. J Therm Anal Calorim. 2008;91:861–6.
14. Jiao CL, Song LF, Jiang CH, Zhang J, Si XL, Qiu SJ, Wang S, Sun LX, Xu F, Li F, Zhao JL. Low-temperature heat capacities and thermodynamic properties of $Mn_3(HEDTA)_2{\cdot}H_2O$. J Therm Anal Calorim. 2010;102:1155–60.
15. Gao CY, Liu SX, Xie LH, Ren YH, Cao JF, Sun CY. Design and construction of a microporous metal-organic framework based on the pillared-layer motif. Cryst Eng Commun. 2007;9:545–7.
16. Li YQ, Xie L, Liu Y, Yang R, Li XG. Favorable hydrogen storage properties of M(HBTC)(4,4′-bipy)·3DMF (M = Ni and Co). Inorg Chem. 2008;47:10372–7.
17. Archer DG. Thermodynamic properties of synthetic sapphire (alpha-Al_2O_3), standard reference material 720 and the effect of temperature-scale differences on thermodynamic properties. J Phys Chem Ref Data. 1993;22:1441–53.